

Chapter 6

Atom–molecule coherence in a Bose-Einstein condensate

6.1 Introduction

The strange time dependence of BEC number loss described in Chapter 5 strongly suggested the presence of non-adiabatic transitions to an undetected molecular state. To further explore this loss process, we utilized a pair of carefully controlled magnetic field pulses, separated in time, in the vicinity of the Feshbach resonance.

The original motivation for the double B-field pulse sequence was to measure the BEC recovery time after a single pulse. We hypothesized that the first pulse would cause a large amount of 3-body recombination-induced number loss to the condensate. The abrupt increase in recombination should produce a multitude of tiny holes or voids in the BEC wavefunction. The sudden creation of voids would lead to condensate excitations because of the localized changes in the mean-field interaction potential [66]. One might ask the question of how long does it take for these voids in the BEC to refill as the surrounding atoms move in. Presumably the condensate recovery time could be determined by applying a second, identical B-field pulse shortly after the first one. One could increase the delay time between pulses until the 2nd pulse produced the same BEC loss as the first pulse; this delay time would define the recovery time and it should give information about the microscopic physics occurring inside the BEC. By measuring the BEC response on such short time scales, one might hope to find evidence for a breakdown in the predictions of mean-field theory.

However, the recovery time picture proved too simplistic. The main defect of this hypothesis lies in its assumption that the BEC number loss is incoherent; in contrast, we actually discovered that a significant part of the loss is due to coherent transfer to another state. We measured coherent oscillations in the BEC atom number as the spacing between the two magnetic field pulses was varied. The observation of coherent oscillations provides us with definitive evidence for coupling between the atomic and molecular states associated with the ^{85}Rb Feshbach resonance. These experiments demonstrate a remarkable quantum superposition between two distinct chemical species: free atoms and weakly bound molecules.

Although the single B-field pulse data from Chapter 5 also suggest that there is nonadiabatic mixing of the atomic and molecular states, these data were not as convincing as the results described here. The experiments discussed in this Chapter have led to a much more accurate theoretical picture of Feshbach resonances; in particular, the physical importance of the shallow s-wave bound state has become clear. As a result of our observations, the phenomenon of atom-molecule coupling and the role of the s-wave bound state in the dynamics of the near-resonant ^{85}Rb BEC have been explored recently by several theoretical groups [56, 16, 67, 68]. A discussion of the present agreement between experiment and theory will be given at the end of the Chapter.

6.2 Experimental methods

To study atom-molecule coherence, we first created ^{85}Rb condensates typically containing 16,500 atoms, with fewer than 1,000 non-condensed thermal atoms. The initial number, N_{init} , fluctuated from shot to shot by ~ 500 atoms ($\sim 3\%$ number noise). After producing a condensate at a B-field of 162.3 G, we ramped the magnetic field adiabatically to 165.5 G, corresponding to an initial scattering length $a_{init} \simeq 7 a_0$. The spatial distribution of the atoms was Gaussian with a typical average atom density of $\langle n_{init} \rangle = 1.8 \times 10^{13} \text{ cm}^{-3}$. For some experiments where a lower initial density was

desired, the adiabatic ramp to 165.5 G was omitted so that the mean field repulsion at 162.3 G ($a_{init} \simeq 200 a_0$) reduced the average initial density to $\langle n_{init} \rangle = 3.5 \times 10^{12} \text{ cm}^{-3}$.

After preparing the condensate, we applied a selected fast magnetic field pulse sequence by sending an appropriate time-dependent current through the auxiliary magnetic field coil. A representative set of double B-field pulses is shown in Figure 6.1. The sequence is composed of two nearly identical short trapezoidal pulses separated by a region of constant magnetic field (B_{evolve}). In our experiments, we varied the evolution time between pulses, t_{evolve} , from 0 to 400 μs , while B_{evolve} ranged from 162 G to 156 G. We determined the value of B_{evolve} between the two pulses using the short rf pulse technique described in section 3.3.3. We also found it useful to alter the initial magnetic field, B_{init} , to change the initial BEC density and distance from the Feshbach resonance. Usually, B_{init} was 162.3G or 165.5 G. We chose the B-field pulse amplitude so that the pulses always approached to within ~ 2 G of the Feshbach resonance.

Upon completion of the fast-pulse sequence in Figure 6.1, we ramped the magnetic field from 165.5 G to ~ 157 G in 5 ms and held the B-field constant for an additional 7 ms to allow the repulsive mean-field energy to expand the condensate (see section 3.5.3). Then we turned off the magnetic trap and used destructive absorption imaging 12.8 ms later to observe the condensate and burst atoms. Our detection scheme was not sensitive to atoms with kinetic energies larger than $\sim 2 \mu\text{K}$ nor to atoms in off-resonant molecular states.

As we observed for single pulses toward the Feshbach resonance, there were two distinct components of atoms visible in the absorption images and a third missing component that we could not detect. One of the observed components was a cold remnant BEC which was not noticeably heated or excited by the fast-pulse sequence (< 1 nK kinetic energy was imparted by the pulse sequence), while the other component was a relatively hot (~ 200 nK) burst of atoms that remained magnetically trapped during the BEC expansion time. Using the PG model to simulate the mean-field expansion that

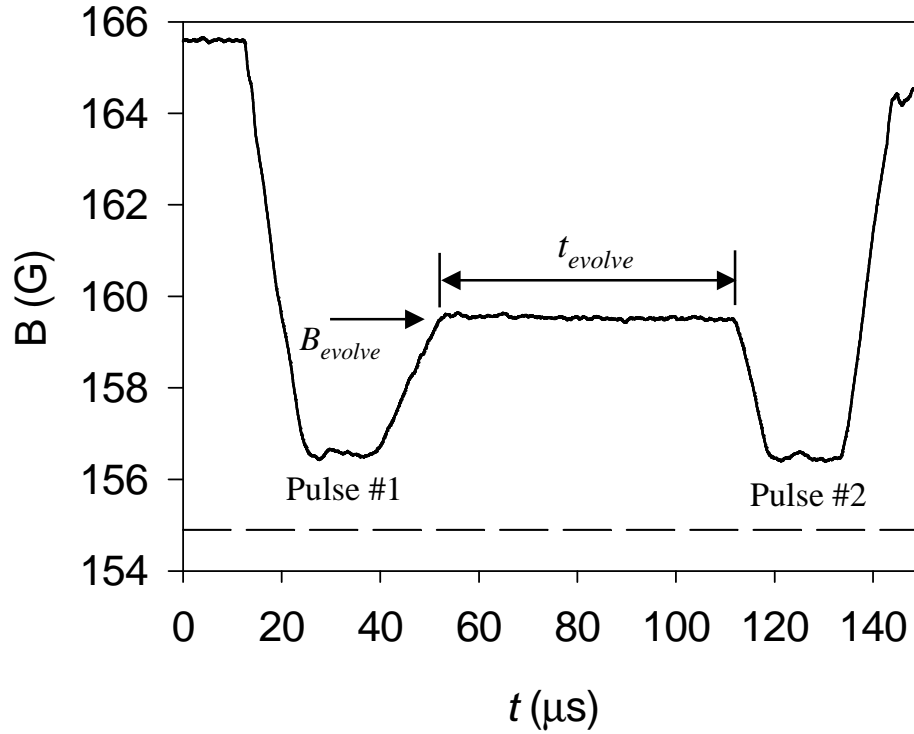


Figure 6.1: Magnetic field pulse shape. B-fields shown for pulses #1 and #2 correspond to scattering lengths of $\sim 3300 a_0$, and the free precession field, B_{evolve} , corresponds to a scattering length of $\sim 600 a_0$. The dashed line indicates the position of the Feshbach resonance, where the scattering length diverges to infinity. In the text, we refer to the free precession time as t_{evolve} . The average ramp time for most of the pulses was $14 \mu\text{s}$.

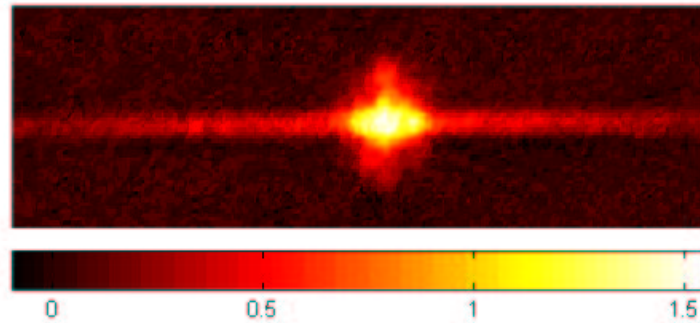


Figure 6.2: An absorption image taken after the fast magnetic-field pulse sequence and the mean-field expansion. The horizontal bar indicates the optical density. The horizontal and vertical directions coincide with the axial and radial axes of the trap, respectively. The dimensions of the image are $366 \times 52 \mu\text{m}$. The BEC remnant is the roughly spherical cloud at the center, while the burst atoms are focused into a thin line along the axial direction. There is a dramatic difference between the two spatial distributions, owing to the large difference in the mean energies of the burst and expanding BEC remnant ($\langle E_{burst} \rangle \simeq 50 \times \langle E_{rem} \rangle$).

we applied to the BEC remnant to measure its number, N_{rem} , we found that we should impart ≤ 3 nK expansion energy to the remnant before imaging. This estimate agrees well with the expansion velocity that we measured after the trap turn-off. Thus the remnant BEC was more than $60\times$ colder than the burst. A typical absorption image of the atoms remaining after the double B-field pulses and time-of-flight expansion is shown in Figure 6.2.

To find the number of atoms in the remnant BEC and the number of burst atoms, we allowed the magnetic trap to focus the burst cloud before imaging. We fit the focused burst (which had a much larger spatial extent than the remnant) with a two-dimensional Gaussian surface, excluding the central region of the image that contained the remnant. This fit yielded the number of burst atoms, N_{burst} . Subtracting the fit from the image and performing a pixel-by-pixel sum of the central region of the image gave the remnant number, N_{rem} .

6.3 Observation of population oscillations

6.3.1 BEC and burst number oscillations versus t_{evolve}

We observed large-amplitude oscillations in the number of BEC and burst atoms as we varied the delay time between magnetic field pulses. Representative number oscillation data for the condensate and burst atoms are displayed in Figure 6.3. The number oscillations were only visible after two B-field pulses; in fact, with only pulse #1 and the subsequent constant B-field but with no pulse #2, N_{rem} showed no variation except for a slow decay. The gradual decay rate of a few atoms per microsecond is consistent with the loss rate expected for a single pulse to the evolution magnetic field, as discussed in Chapter 5. Although we studied the oscillations under a wide variety of different conditions, we never observed the double-pulse value of N_{rem} to be larger than the single-pulse value, implying that each B-field pulse causes some incoherent or

irreversible loss to the BEC.

6.3.2 $N_{missing}$ oscillations

The BEC and burst atom oscillations in Figure 6.3 have very similar amplitudes and frequencies and they appear almost completely out of phase. N_{burst} grows larger when N_{rem} decreases, and vice versa. However, the measured phase shift between the two oscillations is actually $154(4)^\circ$, which is significantly different from 180° . Thus, the BEC and burst number oscillations do not exactly cancel out — if one calculates the total number of atoms, $N_{tot}=N_{rem}+N_{burst}$, this quantity also displays clear oscillations versus evolution time. As shown in Figure 6.4, the amplitude of the N_{tot} oscillations is significantly smaller than that of the other two number components.

Figure 6.4 clearly demonstrates that the time-averaged total number of atoms after the two B-field pulses does not equal the initial number of BEC atoms. There are a number of missing atoms, $N_{missing}$, and the measured oscillations in N_{tot} correspond to oscillations in $N_{missing}$. We therefore have evidence that some of the BEC atoms are oscillating into and out of a *different* state that is not detectable by the experiment. This phenomenon of oscillations to a state that is invisible to the detector may be compared to the well-known neutrino oscillations in astrophysics. We assume that the undetected state in our BEC experiment is the weakly bound molecular state of the Feshbach resonance.

As a side note, the data in Figure 6.4 were measured with fairly low-density condensates to minimize the number of missing atoms that do not oscillate and thereby allow for more atoms in the remnant BEC.¹ This improved the visibility of the remnant and the signal-to-noise ratio for the absorption images. To produce condensates with low density for these measurements, we altered the magnetic pulses somewhat from

¹ We observed that the B-field pulses always produce some missing atoms whose number does not oscillate with t_{evolve} . These atoms may or may not be converted into the weakly bound molecular state. In any case, we found that reducing the BEC density decreased the number of non-oscillating missing atoms. For further discussion of this point, see section 6.4.2.

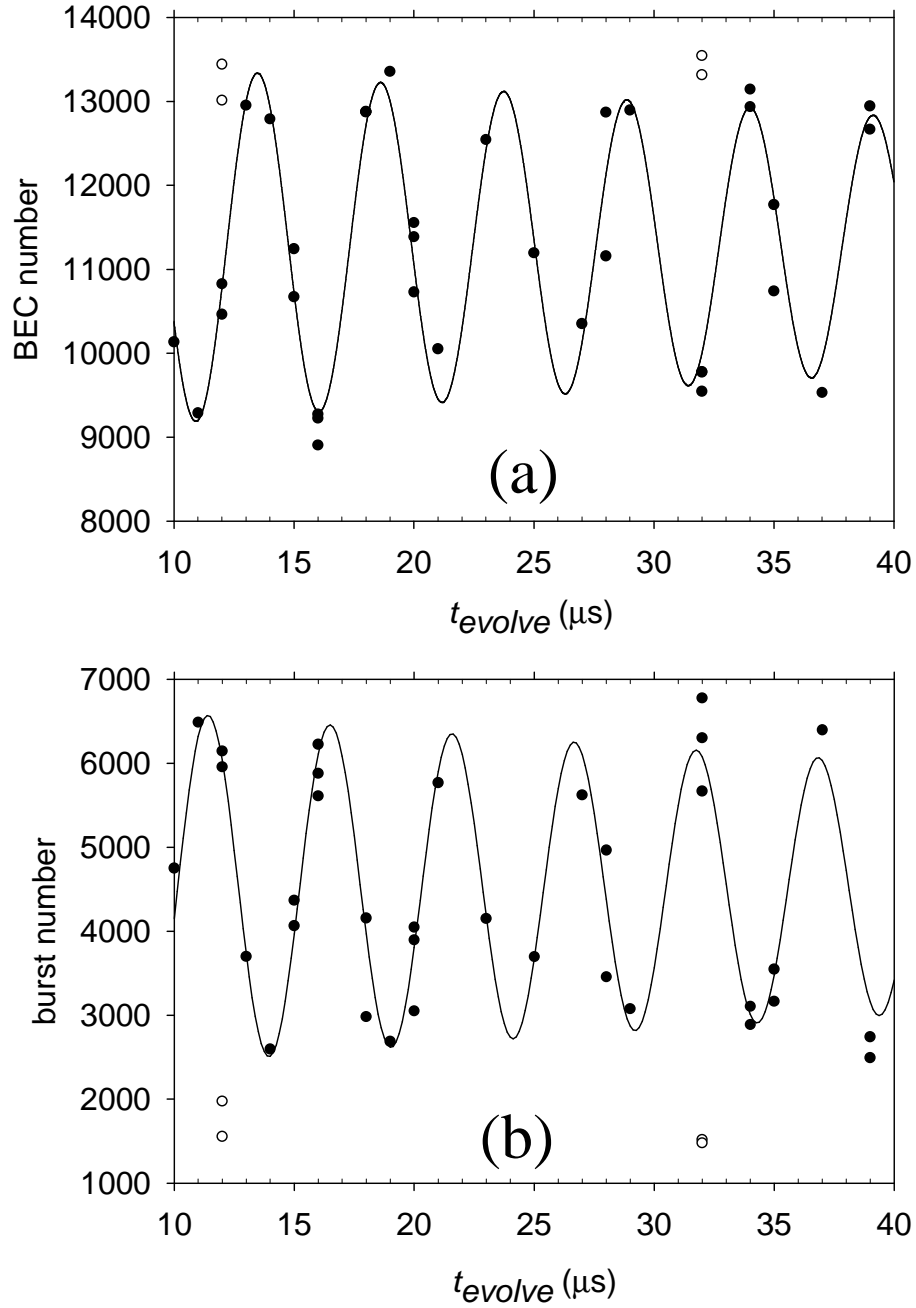


Figure 6.3: Coherent oscillations in BEC number and burst number. **(a)** Black points are the remnant BEC number, N_{rem} , versus evolution time, t_{evolve} , between the two magnetic field pulses. The solid line is a fit to the data using a damped sine wave with a frequency of $196(1)$ kHz and a damping rate of $11(4) \times 10^3 \text{ s}^{-1}$. The open circles near $N_{rem} = 13000$ indicate the number remaining after only pulse #1 and t_{evolve} at 159.84 G. **(b)** Black points are the number of burst atoms versus t_{evolve} . The fit (solid line) yields an oscillation frequency and damping rate that are consistent with those from the fit to the BEC number in part **(a)**. The clear circles are the burst number measured after a single pulse plus a plateau at B_{evolve} . For the data in **(a)** and **(b)**, the initial BEC density was $\langle n_{init} \rangle = 3.5 \times 10^{12} \text{ cm}^{-3}$ and $B_{init} = 162.25(5)$ G. The evolution B-field was $B_{evolve} = 159.84(2)$ G.

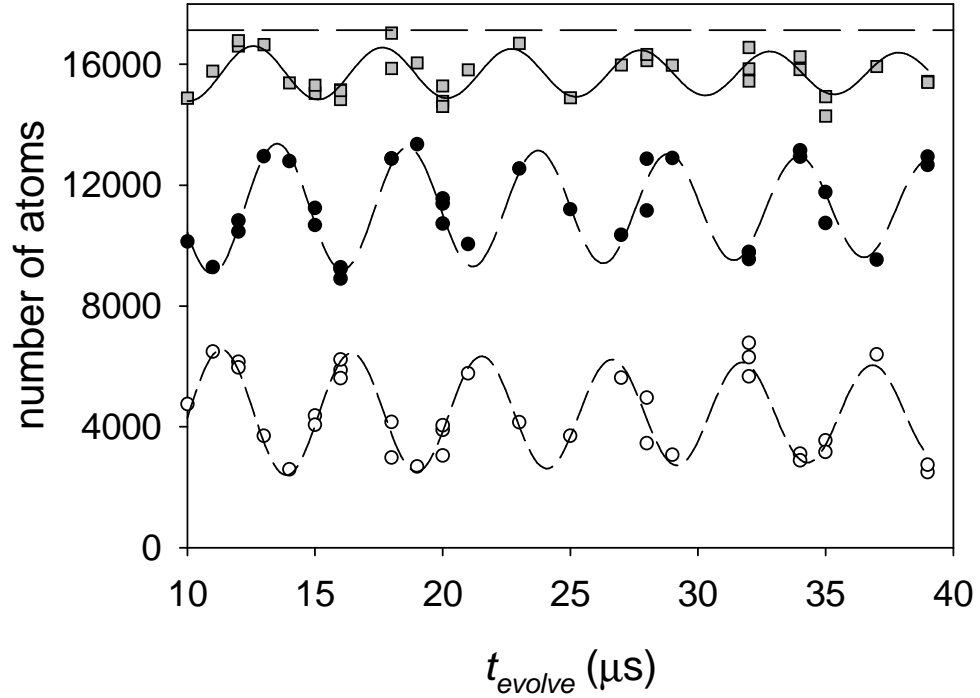


Figure 6.4: Number versus t_{evolve} for low density condensates ($\langle n_{init} \rangle = 3.5 \times 10^{12} \text{ cm}^{-3}$). From bottom to top, the data are N_{burst} (open circles), N_{rem} (filled circles), and the total number of observed atoms (gray squares). Each data set is fit by a damped sine wave as shown by the lines. Here the fitting function is $y = y_0 + A \exp(-t/\tau_{decay}) \sin(2\pi\nu_0 t + \phi)$, where ν_0 is the frequency and τ_{decay} is the decay time constant. The initial BEC number, $N_{init} = 17,100$, is indicated by the flat dashed line. The fit to the BEC remnant data gives an oscillation frequency of $196(1) \text{ kHz}$ and $\tau_{decay} = 91(33) \mu\text{s}$ (the longer time data used to determine τ_{decay} are not shown).

the shapes shown in Figure 6.1. We set the initial magnetic field before the fast-pulse sequence to 162.25(5) G and reduced the amplitudes for pulses #1 and #2 to ~ 7 G. The evolution B-field was $B_{evolve} = 159.84(2)$ G. Under these conditions, the initial BEC density was relatively low: $\langle n_{init} \rangle = 3.5 \times 10^{12} \text{ cm}^{-3}$.

6.3.3 Oscillation frequency versus B_{evolve}

Very strong evidence for the importance of the weakly bound molecular state to the observed BEC dynamics can be obtained from the magnetic field dependence of the number oscillation frequency. We have discovered that the oscillation frequency (ν_0) for the BEC, burst, and missing atom populations matches the binding energy of the molecular state: $h\nu_0 = \epsilon_{\text{bind}}$. We explored the B-field dependence of the oscillation frequency by applying different values of B_{evolve} during the evolution time between the magnetic field pulses. As shown in Figure 6.5, we mapped out ν_0 versus B-field over a ~ 5 G range above the Feshbach resonance field of 155 G. The oscillation frequency varied by almost two orders of magnitude as B_{evolve} increased from 156.6 G to 162 G.

Along with the measured frequencies and magnetic fields, Figure 6.5 also displays theoretical predictions for the molecular bound state energy relative to the atomic state. One prediction, shown by the dotted line, comes from basic zero-energy scattering theory. In the regime where the scattering length is positive and much larger than the radius of the interatomic potential well, the bound state energy for an arbitrary attractive potential can be approximated by $\epsilon = -\hbar^2/ma^2$ [11], where \hbar is Plank's constant divided by 2π , m is the atomic mass, and a is the scattering length. The same equation relates the bound state energy to the effective scattering length, which is calculated from the Feshbach resonance parameters through the relation $a = a_{bg} \times (1 - \frac{\Delta}{B - B_{peak}})$, where a_{bg} is the background scattering length, Δ is the width of the Feshbach resonance, and B_{peak} is the resonant magnetic field. The quantity $|\epsilon|/h$ is plotted with no adjustable parameters in Figure 6.5. The measured oscillation frequencies are in excellent agreement

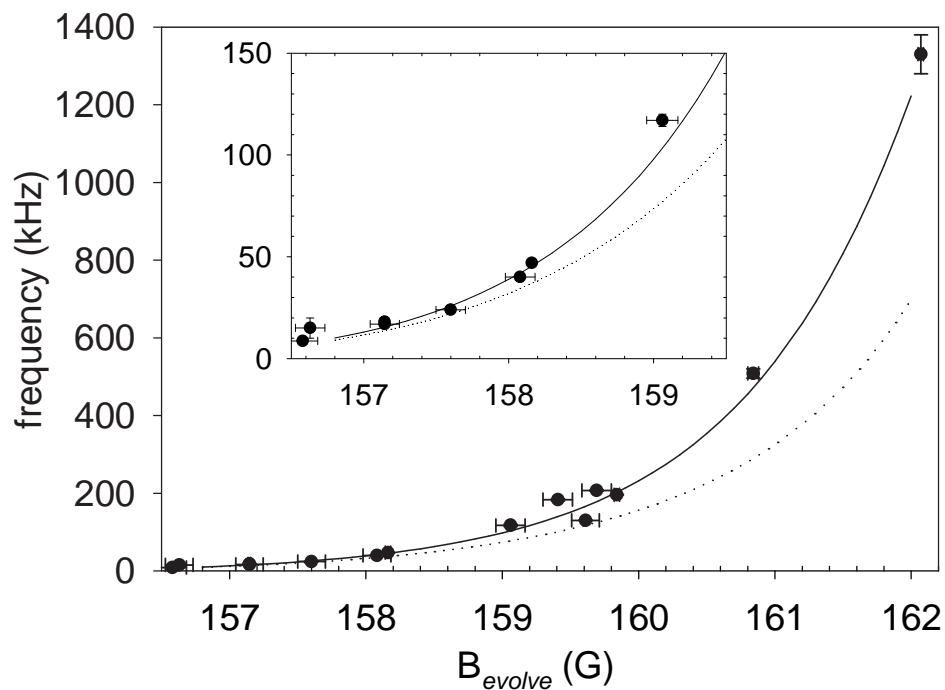


Figure 6.5: Oscillation frequency versus magnetic field. The points are the measured frequencies. The solid line is the energy difference between the atom–atom threshold and the bound molecular state found by S. J. J. M. F. Kokkelmans with a coupled-channels scattering calculation. The dotted line is a plot of $|\epsilon| = \hbar^2/ma^2$. The inset is an expanded view of the lower-frequency data. The magnetic-field measurements for the points with the smallest horizontal error bars were performed on the same days as the corresponding frequency measurements. The error bars for the points with larger field uncertainties were inflated by 100 mG to account for estimated day-to-day field drifts.

with this simple model over the range of magnetic fields where the model is expected to be valid.

The solid line in Figure 6.5 is a prediction of the binding energy from a coupled-channels (CC) scattering calculation by Servaas Kokkelmans. This calculation is based on the results of a recent determination of the rubidium collisional interactions from several high-precision data for ^{85}Rb and ^{87}Rb [69]. We see that the coupled-channels predictions for the binding energy are in excellent agreement with the oscillation frequency data over the entire range of magnetic field. It is important to emphasize that both the simple expression and the more sophisticated CC calculation provide predictions for the binding energy; they are not fits to the oscillation frequency data. The magnetic field dependence of ν_0 is discussed in greater detail in Chapter 7, where we use precision measurements of the frequency and B-field to tightly constrain the parameters of the Feshbach resonance.

6.3.4 Interpreting the oscillations

The fact that the population oscillations occur at exactly the frequency corresponding to the molecular binding energy clearly indicates that we are creating a coherent superposition of atoms and molecules with the sudden magnetic-field pulses. We suggest the following interpretation of our observations. Each magnetic field pulse provides a sufficiently rapid perturbation to result in coherent nonadiabatic transitions between the atomic and molecular states. The first B-field pulse produces an atom-molecule superposition state and the relative phase between the two states in the superposition evolves according to their relative energy difference during t_{evolve} . This energy difference is determined by the B-field-dependent binding energy at B_{evolve} . Because of the relative phase evolution, the final transition probability from the atomic state to the molecular state after the second pulse depends on t_{evolve} . The observed population oscillations are due to a quantum-mechanical interference between the transition am-

plitudes for pulse #1 and pulse #2. Another way to understand the oscillations is to consider that the 2nd pulse transfers some population from the molecular part of the superposition to the atomic state. This “new” probability amplitude in the atomic state can interfere with the amplitude that remained in the atomic state during t_{evolve} . The observed oscillation behavior is somewhat analogous to that seen in Ramsey’s method of separated oscillatory fields [24], in which two microwave pulses, separated in time, drive transitions in a two-level atom.

Although our experiment possesses some similarities to the Ramsey 2-pulse experiment, there are also many differences. It is illustrative to explore these differences. For instance, we observe three distinct components of atoms oscillating as a function of evolution time, each with a different oscillation phase and amplitude. In contrast, the conventional Ramsey oscillations occur in a two-level system where the populations of the two states are always exactly out of phase with one another. An additional difference between our experiment and the Ramsey case is the precise nature of the coupling pulses. In the Ramsey experiment, the two states are coupled by a pair of rf or microwave radiation pulses that are nearly resonant with the transition frequency between the two states. Each radiation pulse has a duration that is much longer than the period of the rf or microwave radiation. Our coupling pulses, on the other hand, involve non-periodic time-variations of a magnetic field. We achieve coupling between the atomic and molecular states by briefly ramping down the relative energy difference between the states toward zero, as in a Landau-Zener experiment. In fact, our experiment is probably best pictured as a combination of Landau-Zener magnetic field coupling pulses separated by a Ramsey-like relative phase evolution between the atomic and molecular states.

The experimentally observed population oscillations in the BEC number indicate that we have produced a coherent superposition of atomic and molecular Bose-Einstein condensates. We propose a simple argument to justify our claim for the existence of

the molecular BEC (mBEC). First, we know from the phase coherence property of condensates that the initial atomic BEC possesses a common phase across the sample of atoms. After the double B-field pulses, we measure large contrast oscillations in the number of BEC atoms, which implies that there is a large fraction of the atomic BEC participating in the population oscillations. If a large fraction of the atomic BEC participates in the oscillations, then the atom/molecule superposition must exist at significantly different spatial positions within the original atomic BEC volume. Thus, we produce molecules that are distributed in space and are phase coherent — these are two important properties that identify a BEC! The creation of a molecular BEC is a remarkable achievement and should provide an abundance of avenues for future study.

6.3.5 Mechanisms for missing atoms

If our interpretation of the BEC number oscillations is correct, then one might ask how it is that we distinguish between the atomic and molecular states. In any interference experiment, there must be some way to discriminate between the two states that are interfering with one another. Since we find that some atoms are missing from the absorption images, we evidently do have a discriminating mechanism that is “built-in” to the experiment.

In our experiment, missing atoms could be created by at least two different mechanisms involving the molecular state. One possibility is that the molecules formed by the double B-field pulses are destroyed when we turn off the magnetic trap and cross the Feshbach resonance. A related idea is presented in Ref. [15]. By turning off the trap, we cause the molecular state to become unbound (the molecular state lies far above the colliding atoms threshold energy for $B=0$). The molecules could therefore dissociate into sufficiently high energy atoms during the trap turn-off ($> 1 \mu\text{K}$) that we would not detect them in the absorption imaging.

Another mechanism for the generation of missing atoms is the possibility of in-

elastic molecule-atom or molecule-molecule collisions during the ~ 30 ms time between the double pulse sequence and the magnetic trap turn-off. In principle the molecules should be confined in the magnetic trap because their magnetic moment is very similar to that of the $|2, -2\rangle$ atomic state for magnetic fields near the Feshbach resonance. During the time that a given molecule resides in the magnetic trap, if the molecule collides with an atom or another molecule, it may drop to a lower energy vibrational level, gaining substantial kinetic energy in the process. In this case, the deeply bound molecule would not experience a Feshbach resonant coupling to the atomic state and the molecule would remain a molecule after the magnetic trap turnoff. However, we would not see the molecule because of its large kinetic energy and low probability of scattering photons from the probe laser. It is important to note that the cross-sections and rates for collisions between highly-vibrationally-excited molecules and ultracold atoms have not been calculated for the heavy alkali atoms [51, 70], although some results have been obtained for He-H₂ collisions [71]. Measuring such a cross-section for Rb₂ would be a major experimental breakthrough.

To investigate the mechanism for missing atom generation, we attempted to measure the number oscillations by imaging the BEC in the magnetic trap. The goal was to look at the BEC immediately after the fast pulse sequence or even during t_{evolve} between the pulses. In theory, the presence or absence of oscillations in the data would then help us to identify how the missing atoms are removed from the sample under our normal operating conditions.

Unfortunately, our attempts to extract useful information from the in-trap imaging of the condensates proved inconclusive. Due to a number of systematic effects related to the small size of the unexpanded BEC, the large Zeeman shift of the trapped atoms, and optical pumping effects that reduce the number of photons scattered by each atom, the absorption images were difficult to interpret. For example, one consequence of not allowing the BEC and burst atoms to expand is the inability to distinguish between the

BEC and burst populations in the images. When we tried to circumvent this problem by expanding the BEC in the trap and then imaging the atoms, the data indicated that the missing atoms were still missing before the trap turn-off. However, this result should be considered preliminary and needs to be confirmed with more data. Although we may return to this experiment in the future, at present we have not definitively determined the mechanism for the missing atoms.

6.4 Controlling the oscillation characteristics

After making some preliminary measurements of the atom-molecule population oscillations, we made a detailed study of the oscillation characteristics. To learn more about the physics of this unique system, we explored the dependence of the oscillations on the initial BEC density as well as the particular shapes of the two magnetic field pulses. The behavior of the atom-molecule oscillations under a variety of different conditions is described in this section.

6.4.1 Amplitude of BEC number oscillations

The first property of the number oscillations that we studied was their amplitude. We desired to increase the amplitude as much as possible, both to increase the number of molecules created and also to improve the signal-to-noise ratio for determining other properties, such as the frequency and phase.

Keeping the pulse lengths fixed at $15 \mu\text{s}$, we varied the double pulse amplitudes to change the approach distance to the Feshbach resonance. For pulses to $\sim 156.3 \text{ G}$, we measured a BEC number oscillation amplitude of roughly 1700 atoms. Increasing the pulse amplitudes to reach $\sim 155 \text{ G}$ caused no change to the oscillation amplitude. The lack of a change is not surprising when one considers that the molecular binding energy has very little B-field dependence from $\sim 156.3 \text{ G}$ to $\sim 155 \text{ G}$ (see Figure 6.5) even though the scattering length increases from $\sim 3000 a_0$ to more than $20,000 a_0$. Since

the magnetic field dependence of ϵ_{bind} is nearly quadratic with B-field to the right of the Feshbach resonance, we expect that the population oscillations should dramatically decrease in amplitude for pulses that only approach to within 3 or 4 G from resonance. We did not attempt to study this expected decrease in oscillation amplitude. We felt that the single pulse data on BEC number loss versus pulse amplitude (see section 5.3) should be adequate for predicting the trend.

Based on the single pulse data for BEC loss, we suspected that varying the pulse lengths of the double pulses could substantially change the amplitude of the population oscillations. Although this proved to be true, nevertheless our original choice of 15 μs for the pulse lengths turned out to produce the largest number oscillations. We studied the pulse length dependence of the oscillation amplitude as the length was increased from 5 μs to 50 μs . The shortest pulses produced very little loss from the condensate, so the oscillation amplitude was small. In contrast, the longest pulses caused huge losses from the condensate (more than 50%), but the oscillation amplitude actually decreased. We found that simply increasing the overall number of missing atoms does not necessarily increase the missing atom oscillation amplitude, implying that there may be two parts to N_{missing} . Some of the loss is coherent and leads to number oscillations while another part of the loss is incoherent. The incoherent number loss grows very rapidly with increasing magnetic pulse length.

6.4.2 Strong density dependence of N_{missing}

In addition to the dependence of N_{missing} on pulse length for the double pulses, we also observed a strong dependence on the initial condensate density. When the BEC density was increased from $\langle n_{\text{init}} \rangle = 3.5 \times 10^{12} \text{ cm}^{-3}$ by more than one order of magnitude, the missing fraction increased from $\sim 8\%$ to $\sim 40\%$ of the initial BEC number. In addition, the number of burst atoms increased dramatically. As a result, the average number of BEC remnant atoms was less than the average number of burst

atoms.

We show the three populations of atoms versus t_{evolve} for high initial BEC density in Figure 6.6. While the burst and condensate numbers apparently still oscillate at the same frequency for these data, the phases and amplitudes of the oscillations in N_{rem} and N_{burst} are such that the total number oscillations are not visible. Under these high density conditions, the number of missing atoms is huge — roughly 10,000 atoms! Here $N_{missing}$ exceeds the average value of N_{rem} , which is about 7000.

We took data similar to those shown in Figure 6.6 for several values of the BEC density and studied the resulting number of missing atoms. To isolate the density dependence of $N_{missing}$, we used fixed values of B_{evolve} and pulse length. We varied the initial density by two different techniques. In the first method, we changed the number of atoms in the BEC by holding the BEC in the magnetic trap for 5 to 10 s after completion of evaporative cooling. Density-dependent losses then reduced the number of BEC atoms without appreciably heating the condensate [1]. Our second method for changing the density was by adiabatically varying the initial magnetic field before the set of double pulses, thereby altering the repulsive self-interaction strength in the condensate. This caused the volume occupied by the BEC ground state wavefunction to vary with the magnetic field. In the latter method, we also adjusted the amplitude of the double pulses to ensure that they maintained the same approach distance to the Feshbach resonance.

The dependence of $N_{missing}$ on BEC density is illustrated in Figure 6.7. Over the range in the plot, the missing fraction rises from nearly zero to 0.4. For some reason, the smooth growth of the missing fraction with density saturates above $\langle n_{init} \rangle \simeq 2 \times 10^{13} \text{ cm}^{-3}$. Further investigation of the missing atoms is needed to understand this trend as well as the origin of $N_{missing}$.

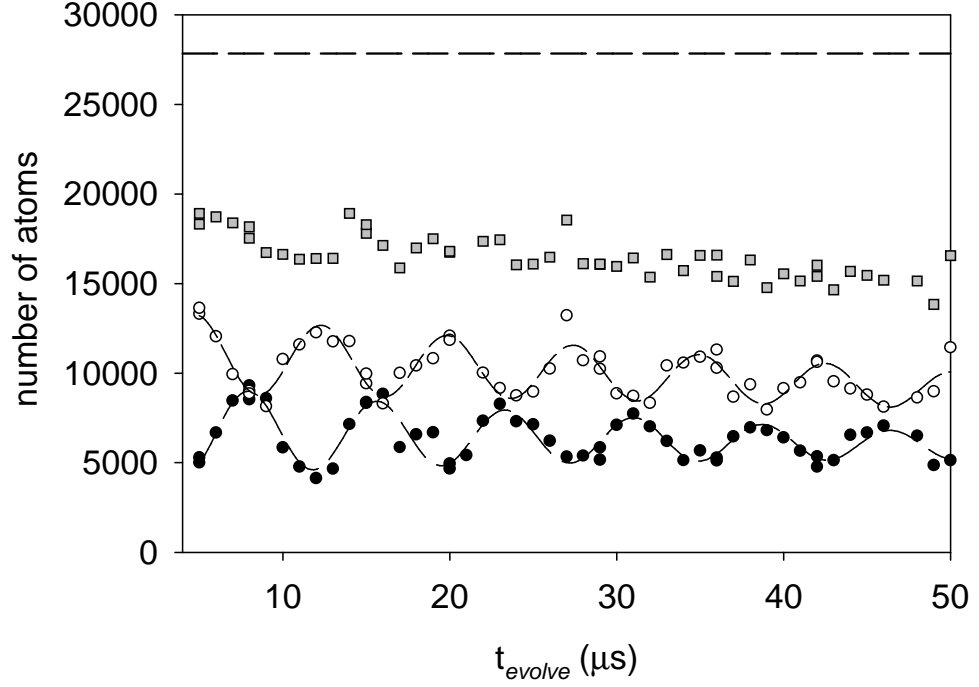


Figure 6.6: Number versus t_{evolve} for high density condensates ($\langle n_{init} \rangle = 4.4 \times 10^{13} \text{ cm}^{-3}$). As in Figure 6.4, we show N_{rem} (filled circles), N_{burst} (open circles), and the total number of observed atoms (gray squares). The lines are damped sinusoidal fits to the different populations of atoms. The initial BEC number, $N_{init} = 27,800$, is indicated by the flat dashed line. The fit parameters for the remnant oscillations are $\nu_0 = 133(1) \text{ kHz}$ and $\tau_{decay} = 38(8) \mu\text{s}$. We added an additional term to the fit function to account for an overall linear loss rate to the number. The fit gave a loss rate of $-19(6) \text{ atoms}/\mu\text{s}$. The evolution B-field was $B_{evolve} = 159.35(5) \text{ G}$. Because the initial magnetic field before the fast-pulse sequence was $165.71(15) \text{ G}$, we used pulse amplitudes of $\sim 10 \text{ G}$ to closely approach the Feshbach resonance.

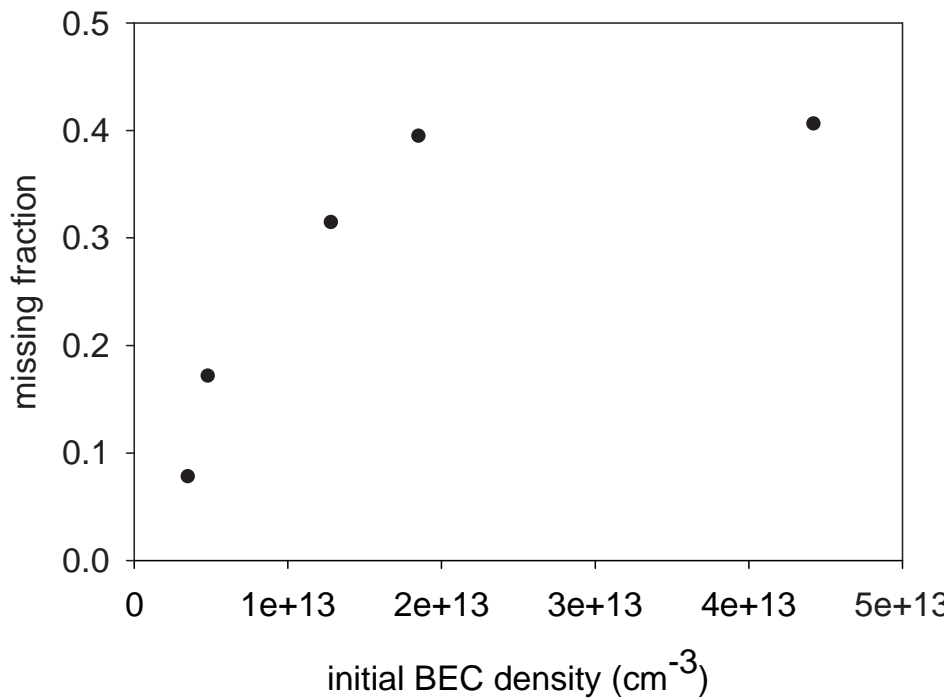


Figure 6.7: Fraction of missing atoms as a function of the initial BEC density. The missing fraction is defined as $1 - \langle N_{total} \rangle / \langle N_{init} \rangle$, where $\langle N_{total} \rangle$ is the average sum of the burst atoms and the BEC remnant atoms and $\langle N_{init} \rangle$ is the average number of BEC atoms before the double pulse sequence. We can determine the density by measuring the initial magnetic field (scattering length) and calculating the volume of the BEC using the PG model. After finding the volume, we use the measured value of $\langle N_{init} \rangle$ to calculate the average density. The typical uncertainty in this density determination is $\sim 20\%$ due to uncertainty in the measured number of atoms and the initial scattering length used in the PG model.

6.4.3 Damping of N_{rem} oscillations

Damping of the number oscillations can be seen in most of the data that we collected. For values of B_{evolve} between 157 G and ~ 161 G, the number oscillations are underdamped, so that the damping time is much longer than the oscillation period. To obtain a high precision measurement of τ_{decay} it is therefore necessary to measure the number oscillations over many cycles. One obvious method to obtain the damping time without requiring too many points is by taking closely-spaced data in windows that are separated by longer time intervals, $\Delta t \gg 1/\nu_0$. Then one can fit the entire set to a damped sine wave that interpolates in the intervals between the data windows.

Unfortunately, we found this method did not work well in practice because of the presence of phase noise in the data. We observed shot-to-shot noise in the oscillation phase for different repetitions of the experimental cycle. The noise was bigger for longer t_{evolve} , indicating that the source of the noise was shifts to the oscillation frequency. The frequency noise was likely due to shot-to-shot magnetic field noise. We provide further discussion of this point in section 7.2.3.

To determine the damping rate despite the presence of phase noise, we adopted another technique for data measurement. We measured N_{rem} versus t_{evolve} in several windows having a length of one or two oscillation periods. The spacing between windows was chosen to be comparable to our estimated $1/e$ time for the damping. We analyzed the data by computing the maximum variation in remnant BEC number within each time window. We plotted ΔN_{max} versus t_{evolve} and fit the data to a decaying exponential function, as shown in Figure 6.8.

We discovered that the damping rate was quite insensitive to both initial BEC density and magnetic field in the B-field range from 157 G to ~ 161 G. Recently, we have found that the rate ($1/\tau_{decay}$) actually increases rapidly as the magnetic field increases above ~ 161 G, which is possibly related to the rapid variation in binding energy with

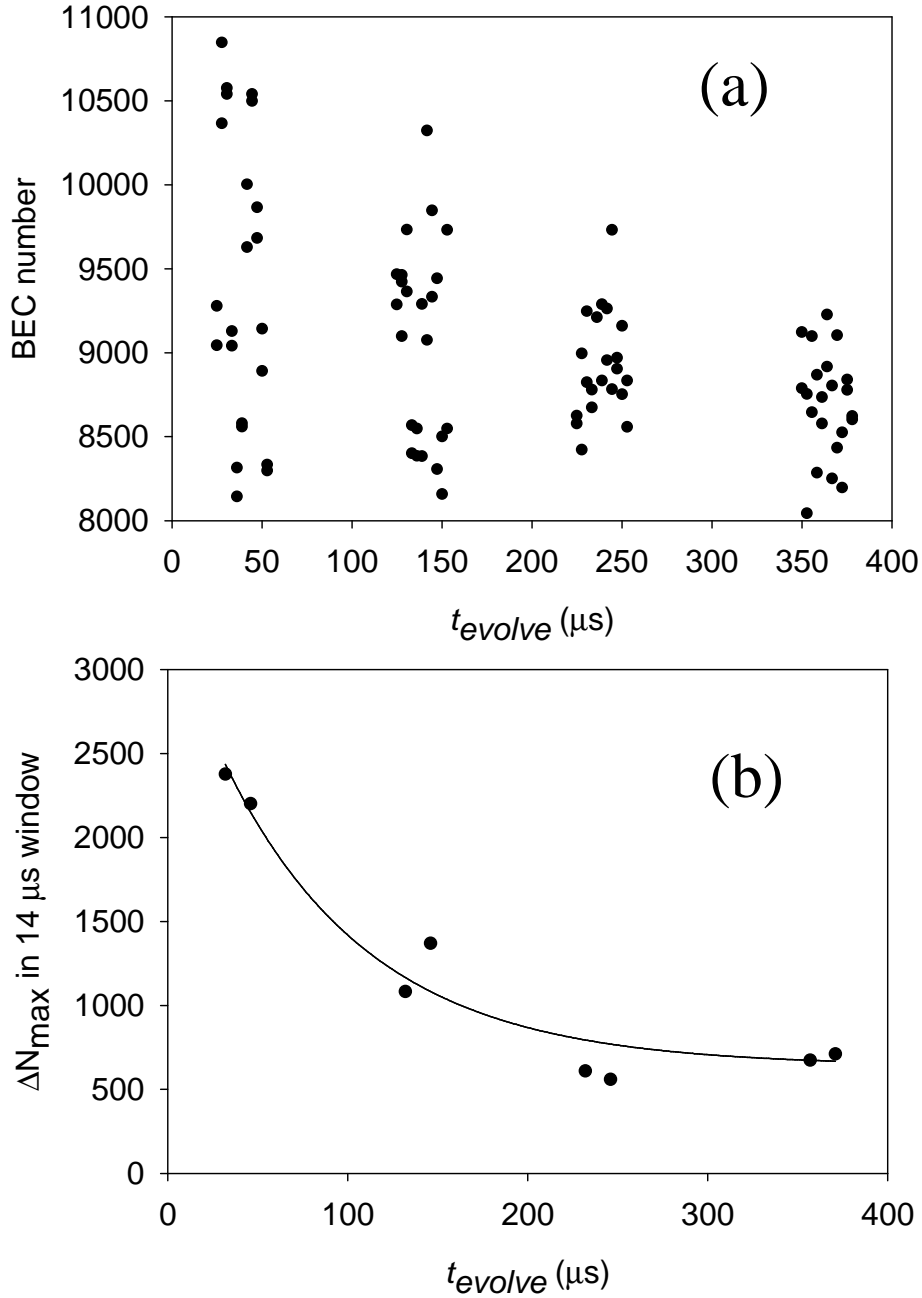


Figure 6.8: Damping of BEC number oscillations. (a) BEC remnant number (N_{rem}) versus t_{evolve} . The data are grouped into 4 windows with each window consisting of 2 oscillation periods. (b) Peak-to-peak variation in remnant number, ΔN_{max} , versus t_{evolve} (black points). ΔN_{max} is calculated for a single oscillation period, which is roughly $14 \mu\text{s}$ in length. The line is an exponential decay fit to the data, with the baseline fixed at the average of the four longest time data: $N_{base}=640$ atoms. The damping time from the fit is $82(14) \mu\text{s}$ (damping rate $\gamma = 12(2) \times 10^3 \text{ s}^{-1}$). The baseline of 640 atoms is quite reasonable considering the peak-to-peak number noise observed during the measurement. Note that the peaks of the oscillations in part (a) decrease more rapidly than the troughs due to an overall loss of BEC atoms during t_{evolve} . We find that the loss is linear with time and occurs at a rate of $-2.2(2) \text{ atoms}/\mu\text{s}$.

magnetic field. Both the B-field dependence and possible mechanisms for the damping are presently under investigation and will be the subject of a future publication by our group.

We also looked for a temperature dependence of both the damping and the oscillation frequency at $\nu_0 \sim 200$ kHz and did not see any. The high-temperature data were much noisier than the data for pure condensates, due to unexplained enhanced noise in the number of thermal atoms after the magnetic field pulses, but when the initial thermal fraction was increased from $<5\%$ to 30% , the data still displayed oscillations with frequency, amplitude, and damping consistent with what was observed with low temperature data. Since we changed N_{therm} by more than a factor of 6 and saw no effect, any dependence of the damping rate on temperature must be very weak.

6.4.4 Relative phase between N_{rem} and N_{burst} oscillations

A particularly intriguing aspect of our data is the observation of three distinct oscillations in the various number components visible from the absorption images. Because the relative phase between the BEC remnant and the burst oscillations does not equal 180° , there is a third oscillation visible in $N_{missing}$ (or N_{total}). We believe that the $N_{missing}$ oscillation amplitude may correspond to the number of molecules produced by the double pulse sequence.

For reasons that will be elucidated later in this section, we suspected that the number of molecules might be increased by ramping the B-field more slowly at the end of magnetic field pulse #2. We therefore examined the amplitude of the $N_{missing}$ oscillations as a function of the final ramp time of the second B-field pulse. As a result of changing this ramp time, there were variations in the relative phase between the BEC remnant and burst number oscillations, $\Delta\phi = \phi_{burst} - \phi_{BEC}$. The relative phase variations caused the $N_{missing}$ oscillation amplitude to change significantly. For example, increasing the final ramp time of pulse #2 from our default value of $11 \mu s$ to

160 μs caused the missing number oscillation amplitude to increase from 1000 atoms to nearly 2800 atoms. The number oscillations for the 160 μs final ramp time are displayed in Figure 6.9.

By comparing different data sets such as those shown in Figure 6.9, we observed that the relative phase shift, $\Delta\phi$, decreased as the final ramp time for pulse #2 became longer. The phase shift behavior was entirely due to a phase shift in the burst number oscillations; the BEC remnant phase remained fixed. As the final ramp time increased, the burst oscillation phase shifted in such a way that the lowest curve in Figure 6.9 moved smoothly to the right. We show the quantitative details of this trend in Figure 6.10. There $\Delta\phi$ is seen to decrease from $\sim 150^\circ$ to $\sim 80^\circ$ as the ramp time goes from 10 μs to 330 μs . After an initially rapid decline, the relative phase eventually levels out for slower and slower ramps.

After demonstrating that the relative phase shift could take on values very different from 180° , we scratched our heads and wondered about the origins of the shift. Since we had generally observed that fewer atoms in the BEC correspond to more atoms in the burst, we speculated that the phase shift between the N_{rem} and N_{burst} oscillations might originate in a time delay between the disappearance of the BEC and the creation of the burst atoms. To determine whether $\Delta\phi$ was a true phase shift or was simply a shift caused by a fixed time delay, we measured $\Delta\phi$ at two different values of the oscillation frequency. While holding the pulse #2 final ramp time fixed at 160 μs , we changed B_{evolve} to alter the oscillation frequency. Decreasing ν_0 from ~ 200 kHz to 56 kHz caused the relative phase shift to change from $68(7)^\circ$ to $88(9)^\circ$. The relative phase shift therefore increased by a factor of 1.3(2). However, if the phase shift were due to a fixed time delay, then decreasing the frequency by a factor of 4 should cause $\Delta\phi$ to drop by a factor of 4 also (so we would expect $68^\circ/4 = 17^\circ$ in this case). Thus, the time delay idea is clearly not correct.

Nevertheless, it remains true that the second magnetic pulse shape affects the

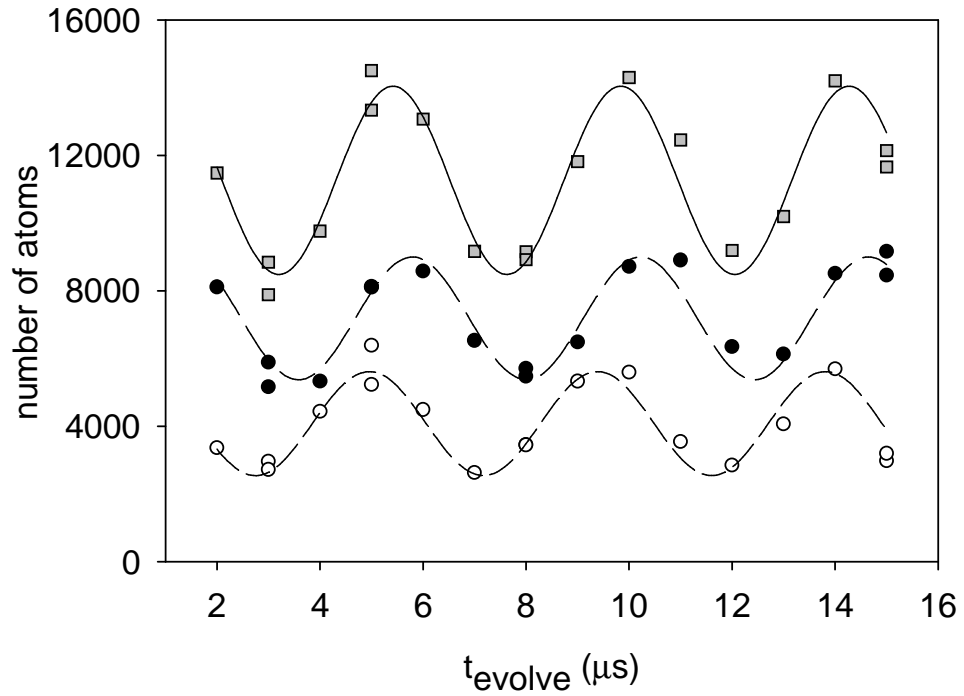


Figure 6.9: Enhanced N_{missing} oscillations. Number versus t_{evolve} for a relatively long pulse #2 final ramp time of $160 \mu\text{s}$. From bottom to top, the data are N_{burst} (open circles), N_{rem} (filled circles), and the total number of observed atoms (gray squares). The different data sets are fit by damped sine waves as shown by the lines. The relative phase between burst and remnant oscillations is $\phi_{\text{burst}} - \phi_{\text{BEC}} = 68(7)^\circ$, which is more than $2\times$ smaller than the $147(8)^\circ$ phase difference for our typical $11 \mu\text{s}$ final ramp time (see Figure 6.4 and related discussion in the text).

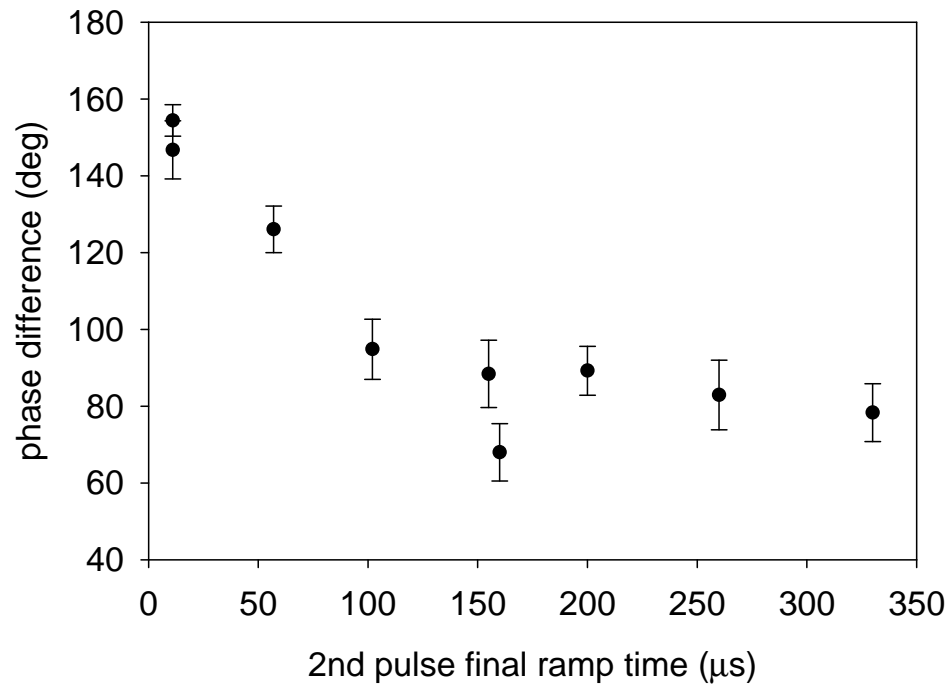


Figure 6.10: Relative oscillation phase versus final ramp time of 2nd B-field pulse. Black points with error bars are the phase difference $\phi_{burst} - \phi_{BEC}$. To calculate the phase difference, we first fit each population oscillation (remnant BEC atoms, burst atoms, and total number of atoms) to a sinusoidal function. From these three fits, we then compute the weighted average oscillation frequency. We next fit each component of atoms again, constraining the oscillation frequency for the fit to be equal to the weighted average value. This procedure allows us to determine the phase shift between the burst and remnant BEC number oscillations with improved precision.

ratio of BEC atoms to burst atoms at fixed evolution time. For instance, if we choose t_{evolve} such that N_{rem} is at a minimum or trough of the oscillation, then lengthening the 2nd pulse final ramp time causes the number of burst atoms to decrease and the missing number to increase. Another way to see this is to compare the phases of the oscillations in N_{rem} and $N_{missing}$. As the final ramp time becomes longer, the remnant oscillations become more and more out of phase with the missing number oscillations. Concurrently, the amplitude of the $N_{missing}$ oscillation grows larger.

These observations suggest that we preserve more molecules (more missing atoms) after pulse #2 by slowing down the final ramp. We believe that increasing the 2nd pulse final ramp time enhances the probability that the molecules formed during the coupling pulse survive the ramp back toward higher B-field (~ 166 G). The justification for this claim is based on the arguments of Chris Greene and Murray Holland. Since the radial wavefunction of the weakly bound molecular state has a size characterized by the scattering length (see Chapter 2), a longer pulse should allow a more gradual or adiabatic decrease in the size of the wavefunction toward smaller and smaller radius. In contrast, the shorter ramp times are more sudden and they lead to a higher probability that the molecule will simply dissociate into a pair of free atoms during the ramp. It is possible that the hugely extended molecules that are created near the Feshbach resonance are very fragile and they dissociate when the B-field jumps quickly back to small a . If this interpretation is correct, then the data imply that the dissociation of the molecular state can be influenced by the magnetic field ramp rate — with slower ramps leading to less dissociation.

One must take some care when talking in this way about the state of the molecule at a particular B-field (scattering length) because of the time variation of the field. During the double magnetic field pulses, the state of the system is far from equilibrium. We only observe the populations of the BEC remnant and burst atoms long after the atom-molecule coupling dynamics have ended.

While the “fragile molecule” hypothesis discussed above appears to have some validity, it is far too simple to describe all of the effects of changing the ramp time of pulse #2. In addition to the relative oscillation phase shifts and the oscillation amplitude of $N_{missing}$, we observed that several other observables depended on the 2nd pulse final ramp time. For example, the oscillation amplitude of N_{rem} and N_{burst} exhibited a slight decrease as the final ramp lengthened. There was also a decline in the average energy of the burst atoms for slower ramps. These trends have not been explained at the present time.

6.4.5 Burst energy oscillations

The final feature of the atom-molecule coherence experiments that we describe in this Chapter involves the energy of the burst atoms. We measured a periodic modulation of the average energy of the burst atoms as a function of t_{evolve} , as shown in Figure 6.11. The data in the Figure are the average energies corresponding to the burst atom number data that was plotted previously in Figure 6.6. For these data, number of burst atoms was the highest we ever observed, so that $N_{burst} > N_{rem}$. The large number of burst atoms in the absorption images facilitated the determination of the average energy of the distribution along the axial direction. As described in section 5.2.3, we fit each burst atom distribution to a 2-D Gaussian function and used the width of the Gaussian in the long dimension to calculate the average energy. In Figure 6.11, the observed variation in energy of ~ 50 nK is equivalent to a modulation of ~ 17 μm in the rms width of the focused burst atom cloud. The energy oscillations appear to damp out fairly rapidly until they become lost in the noise after ~ 35 μs . Our measurements show that both the number of burst atoms and their energy distribution change with t_{evolve} .

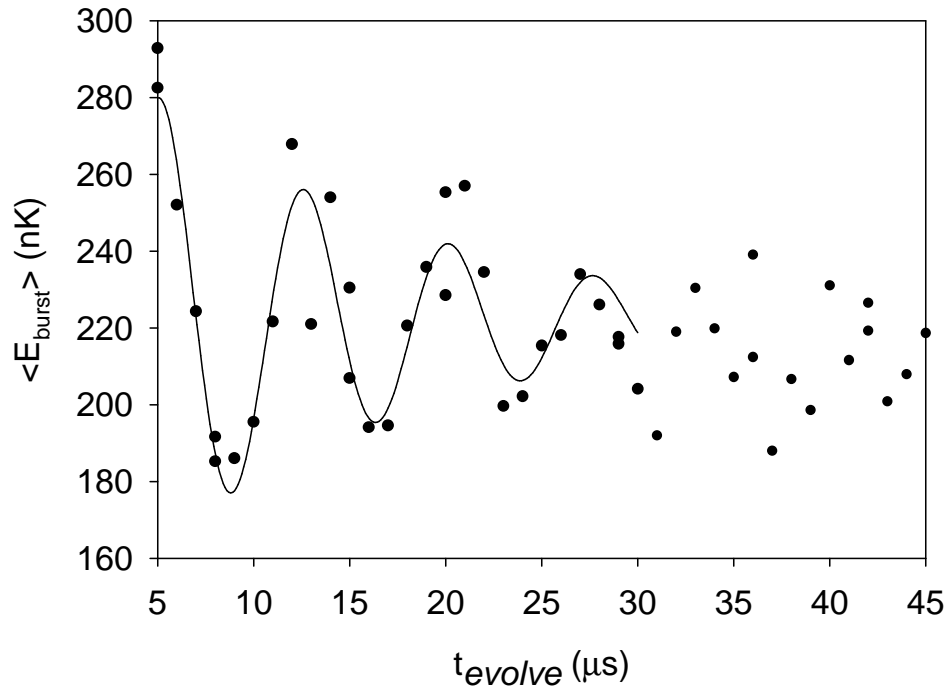


Figure 6.11: Average axial burst energy versus t_{evolve} . Black points are the average axial burst energy at different values of the evolution time between the double pulses. The line is a damped sine wave fit to the data for $t_{\text{evolve}} \leq 30 \mu\text{s}$. The fit yields the parameters: 222(2) nK average energy, 83(15) nK oscillation amplitude, 133(3) kHz oscillation frequency, and $70(16) \times 10^3 \text{ s}^{-1}$ damping rate. The oscillations in the average energy occur at the same frequency and phase as the burst number oscillations (see Figure 6.6), while the damping of the energy oscillations is roughly $3\times$ faster than in the burst number oscillations.

6.5 Discussion of theoretical models

The observations of atom-molecule coherence described in this Chapter raise a number of outstanding questions. First, do the magnetic field pulses really produce molecules and if so, do the molecules form a molecular BEC? As discussed in section 6.3.4, the fact that we see an oscillation involving a large fraction of the atomic BEC strongly supports the existence of a molecular BEC. There are many remaining questions, however. For instance, exactly how many molecules can we produce and how can we increase this number by optimizing the shape of the B-field pulses? Another outstanding issue is the precise relationship between the burst atoms and the molecular state. Finally, what happens to the molecules after they are created? Are there collisions and/or mean-field interactions with the surrounding atoms [72]?

For a definitive experimental answer to these questions, we need to devise a method to directly detect the molecules and their spatial distribution in the magnetic trap. New experiments are currently being developed at JILA that should allow molecule detection by photo-ionization and subsequent detection of the molecular ions. However, many useful insights and possible answers to the questions raised by our data can be obtained from recent theoretical work. A number of theorists [9, 16, 67, 73, 68], inspired by our oscillation data, have studied the ^{85}Rb BEC system. Some of the theorists have developed models that capture most of the prominent experimental features, especially the existence of the different oscillating components of atoms that we observe. We describe the successes of some of the relevant theories in this section. We also point out areas that remain unexplored theoretically. At the end of the section, we use a table to present a concise comparison of the theories to the relevant experimental observables.

6.5.1 Kokkelmans and Holland model

Kokkelmans and Holland's theoretical description of the atom-molecule coupling experiments [9] was briefly described in Chapter 5. The authors emphasize that it is very important to properly incorporate the two-body scattering physics into their effective quantum field theory. The Feshbach resonance in the two-body atomic scattering can be described most accurately by a coupled-channels calculation, which predicts the B-field-dependent scattering length, the binding energy of the molecular state, and the bound state wavefunction (see Chapter 2). Kokkelmans and Holland show how to include the complex scattering physics into a simple effective Hamiltonian used in mean-field theory [56]. This effective Hamiltonian can then be used to predict the response of a near-resonant condensate to variations in magnetic field.

Kokkelmans and Holland solve a set of time-dependent equations for their effective Hamiltonian, which depends on magnetic field. Using the experimental B-field pulses, they integrate the equations for a homogeneous BEC. To model the inhomogeneous density distribution of the real condensates, Kokkelmans and Holland conduct their calculations for a range of densities, finally performing a Gaussian weighted average of their results. This corresponds to a local density approximation for the BEC. The authors assert that they can safely ignore any other physics due to the trapping potential because of the short time duration of the magnetic field pulses (much shorter than the magnetic trap oscillation period).

The theory successfully predicts a number of details of the experiment. Kokkelmans and Holland identify the condensate remnant as the atomic BEC field in their theory, while the burst atoms of the experiment correspond to noncondensate atoms that are created in strongly correlated pairs. The missing atoms are identified as a molecular BEC. Kokkelmans and Holland suggest that the reason the molecules turn into missing atoms in the experiment is because of inelastic collisions with BEC atoms

before the magnetic trap turn-off.

For a double pulse sequence beginning at $B_{init}=162$ G (low initial BEC density), the Kokkelmans/Holland theory predicts striking oscillations in the number of BEC and burst atoms, with an oscillation frequency that matches the binding energy of the molecular state. In the theoretical results, there is a phase shift between the remnant and burst oscillations that agrees with the experiment. In addition to these predictions, Kokkelmans and Holland find that the average energy of the burst atoms is similar to that observed experimentally.

There are only two important aspects of our experimental data that are not described by this theory. First, the theory does not contain any mechanism to cause the large numbers of non-oscillating missing atoms that we observe. We found in section 6.4.2 that increasing the BEC density caused the average value of $N_{missing}$ to increase dramatically. These missing atoms may be removed from the BEC by 3-body recombination, which is not contained in the Kokkelmans/Holland model. In the recombination process, two atoms spontaneously form a molecule during a collision with a third atoms. An alternative explanation to the recombination idea is that the non-oscillating missing atoms are in fact coherently formed molecules, but the Kokkelmans/Holland theory fails to predict their presence. An additional feature of the experiment that is not explained by the theory is the strong dependence of the relative phase, $\Delta\phi$, between burst and BEC remnant oscillations, on the final ramp time of the second B-field pulse. While Kokkelmans and Holland did observe a such a dependence, it was much weaker than in the data. Since we have interpreted the relative phase variation in terms of making more molecules, it would be interesting to further study the trend in the context of the Kokkelmans and Holland theory.

Overall, the success of this theory is remarkable. The Kokkelmans/Holland theory provides an explanation of the burst atoms — they are noncondensate atoms that develop strong pair correlations due to the B-field ramps near the Feshbach resonance.

According to the model, the burst atoms significantly outnumber the molecules due to the large spatial overlap of the weakly bound molecular state with the pairing field that describes the two-body correlations. For the B-field pulse and initial BEC density used in Ref. [9], the molecular fraction is predicted to be much smaller than the burst — only $\sim 2\%$ compared to $\sim 25\%$. In addition, the authors identify the oscillating population of missing atoms as a molecular BEC.

6.5.2 Kohler, Gasenzer, and Burnett model

Another theoretical paper describing our ^{85}Rb BEC experiments was recently produced by the theory group at Oxford [16]. In this work, Kohler, Gasenzer, and Burnett utilize a generalization of the mean-field theory leading to the well-known Gross-Pitaevskii equation. The theory goes beyond the GP equation by including first and second-order correlations between the atoms. This leads to a nonlinear Schrodinger equation for the atomic mean field (atomic BEC). The Schrodinger equation describes the relative motion of two colliding atoms through a time evolution operator. The operator and its related coupling function capture the full time-dependence of the magnetic field or scattering length in the experimental B-field pulses. The authors of Ref. [16] assert that their microscopic dynamics approach avoids any assumptions about the type of states involved in the system of colliding BEC atoms. They determine the state of the atoms after a double pulse sequence by projecting onto a given set of basis states, but the results are not dependent on the choice of the states. In addition, Kohler, Gasenzer, and Burnett examine the effect of including the magnetic trap potential. They compare their results for both a homogeneous gas and a trapped gas to learn more about the physics of the atom-molecule coupling.

Like the Kokkelmans/Holland effective field theory, the model of Ref. [16] predicts oscillations in the number of BEC atoms as a function of t_{evolve} between a pair of magnetic field pulses toward the Feshbach resonance. Kohler, Gasenzer, and Burnett

also identify a relatively hot component of noncondensate atoms in their theory with the burst atoms observed in the experiment. A population of bound molecules exists after the B-field pulses as well; according to the authors, these bound molecules correspond to the missing atoms in the experiment (no consideration is given as to how the molecules actually become missing atoms). The properties of the weakly bound molecular state near the Feshbach resonance are explored by the authors of Ref. [16] in a useful appendix to the paper.

For the case of a homogeneous BEC subject to a set of B-field pulses similar to those used in the experiment, the theory predicts that the BEC and burst populations oscillate slightly out of phase with one another, so that their sum, N_{total} , also oscillates. The amplitude of the N_{total} oscillations is reduced relative the that of the BEC and burst numbers, as was seen in experimental data.

When Kohler, Gasenzer, and Burnett include the magnetic trap in their simulations, they observe the same qualitative behavior in the number oscillations, but there are significant quantitative differences. The average number of burst atoms and missing atoms is seen to depend strongly on the presence of the trap potential. For instance, adding the trap potential causes the average burst fraction to increase from $\sim 15\%$ to $\sim 40\%$ while the average missing fraction decreases from $\sim 10\%$ to $\sim 5\%$. However, the phases and frequencies of the population oscillations remain unchanged when the magnetic trap is included in the Schrodinger equation. The authors of Ref. [16] explain that the dependence of the quantitative details of the oscillations on the presence of the trap potential arises from the first B-field pulse toward the Feshbach resonance. During this pulse to 155.5 G, the magnitude of the scattering length approaches the harmonic oscillator length of the trap, which strongly affects the interactions of the atom pairs. Since the oscillator length does not appear in the homogeneous theory, it seems reasonable that the results should depend somewhat on the inclusion of the trap potential.

One interesting aspect of the theory is its explanation of the origin of the burst

atoms. The authors of Ref. [16] point out that the magnetic field pulses provide energy for the relative motion of the noncondensate atom pairs, but there is no transfer of momentum. Thus, the center-of-mass motion of the burst is unaffected by the magnetic field ramps.

In addition to providing energy for the relative motion of the burst atoms, the time-dependent B-field can remove energy from the system so that atom pairs can become bound together. Kohler, Gasenzer, and Burnett also predict the formation of a molecular BEC due to the B-field pulses. The authors state that after the pulse sequence, the mBEC remains overlapped with the atomic BEC while the burst atoms undergo a ballistic expansion. A density distribution for the molecular BEC is given in the paper.

There are some results of the experiments in this Chapter that remain unexplained by the Kohler, Gasenzer, and Burnett model. The large, density-dependent fraction of missing atoms that do not show an oscillating population are not predicted by this model. In addition, there is no modeling of our observed phase shift dependence on second B-field pulse final ramp time. Presumably this could be done and compared to data to further test the applicability of the theory; however, as in the model of Ref. [9], heavy numerical work is required to evaluate the predictions of the Kohler, Gasenzer, and Burnett theory. It is difficult for experimentalists to apply this model to the data to gain further intuition about the observed trends. For instance, we would like to use one of these successful theoretical models to investigate the dependence of the $N_{missing}$ oscillation amplitude on the second pulse final ramp time. Of course, it is not really fair to complain that the theory is too complicated because an accurate description of the physics probably does require an effective field theory.

6.5.3 Overview of experiment and theory

To clarify the comparisons between theory and experiment described here, we summarize them in Table 6.1. Here we list the experimental observables and trends and a brief note on the current status of agreement with theory.

Table 6.1: Comparison of experimental observables and trends with the two theoretical models described in this section.

Observation	Kokkelmans/Holland	Kohler/Gasenzer/Burnett
N_{rem}, N_{burst} osc. amplitude	calculated; agrees with expt.	calculated; agrees with expt.
$\langle N_{rem} \rangle, \langle N_{burst} \rangle$ avg. values	calculated; agrees with expt.	calculated; agrees with expt.
$N_{missing}$ oscillations	calculated; agrees with expt.	calculated; agrees with expt.
$\Delta\phi = \phi_{burst} - \phi_{BEC} \simeq 150^\circ$	calculated; agrees with expt.	calculated; agrees with expt.
$\Delta\phi$ vs. $t_{ramp, final}$ of pulse #2	calculated; does not agree	not yet calculated
$\nu_{osc} = \epsilon_{bind}/\hbar$	calculated; agrees with expt.	calculated; agrees with expt.
Damping of N_{rem} osc.	not yet calculated	not yet calculated
$N_{missing}$ vs. $\langle n_{init} \rangle$	calculated; does not agree	not yet calculated
$\langle E_{burst} \rangle$	calculated; agrees with expt.	calculated; agrees with expt.
$\langle E_{burst} \rangle$ oscillations	not yet calculated	not yet calculated

In addition to the theoretical models described here, there are several other papers that study the atom-molecule coupling in ^{85}Rb [67, 73, 68]. In particular, the predictions of Mackie et al. [67] bear some similarities to the observations of the experiments. However, the agreement is not particularly good. Since the Kokkelmans/Holland and Kohler, Gasenzer, and Burnett models have been so successful in describing our experiments, we do not include discussion of the other theories here.